Applicability of AC impedance method for measuring time-variant corrosion rate to cracked and crack-repaired reinforced concrete

Toshinori Kanemitsu (kanetosh@criepi.denken.or.jp)
Central Research Institute of Electric Power Industry https://orcid.org/0000-0001-8659-4038
Satoshi Takaya
Kyoto University Faculty of Engineering Graduate School of Engineering: Kyoto Daigaku Kogakubu Daigakuin Kogaku Kenkyuka

Research Article

Keywords: AC impedance method, Corrosion rate, Crack, Crack repair, Accelerated corrosion environment

Posted Date: March 8th, 2022

DOI: https://doi.org/10.21203/rs.3.rs-1401939/v1

Version of Record: A version of this preprint was published at Materials and Structures on January 24th, 2023. See the published version at https://doi.org/10.1617/s11527-023-02108-w.

Abstract

Purpose Several models of the time-variant corrosion rate (CR) have been proposed to predict the service life of reinforced concrete (RC) structures based on polarization resistance (PR) monitoring. However, few of them have verified the accuracy by comparing the estimated corrosion weight loss (CWL) obtained from the PR monitoring with the actual CWL. In addition, few studies have measured the time-variant CR on crack-repaired RC specimens, and the evaluation of repair efficacy is clearly an essential step in the maintenance of the structures. This study aims to clarify the applicability of the alternating current (AC) impedance method, one of the PR methods, to cracked and crack-repaired RC. Methods The CRs in such RC in an accelerated corrosion environment were measured every one to three months over three years using the AC impedance method. To confirm accuracy, the corroded area and CWL of the steel bars were measured. Results The results clarify that the measurement area of the AC impedance method was almost equal to the corroded area, which indicates that the corrosion area should be calculated in addition to the CWL for accuracy verification. The results also show that the AC impedance method can be applied to cracked and crack-repaired RC for measuring time-variant CR. Conclusion The CR increases rapidly after crack initiation but becomes constant with time, and early crack repair can delay corrosion progress in cracked RC to the same extent as in uncracked concrete.

1. Introduction

In recent years, the number of aging reinforced concrete (RC) structures has been increasing, and the need has arisen for efficient repair and reinforcement measures to extend the service life at a low cost. RC structures near the sea particularly tend to deteriorate rapidly owing to contact with chlorides via direct seawater or seawater splashing, while deicing agents made of calcium chloride can also be a potential source of chloride. Steel corrosion in concrete occurs when the chlorides penetrate the concrete and reach the steel bar. The bar diameter is decreased due to the corrosion progress, which in turn decreases the load resistance of the RC structure. Therefore, it is crucial to measure the time-variant corrosion rate (CR) of steel bars in concrete to predict the service life of the structure.

Some studies have proposed prediction models of CR based on various environmental conditions, material properties, and exposure time before crack initiation [1–7]. Environmental conditions include chloride ion content, humidity, and temperature, and material properties include the water–binder ratio (W/B), binder type, and concrete cover thickness on the steel. The CR also decreases with time because corrosion products gradually form in an interfacial transition zone between steel bars and concrete [2, 4, 5].

Evaluation of the time-variant CR after cracking is becoming increasingly important. Steel corrosion in concrete may accelerate owing to bending cracks induced by mechanical causes such as earthquakes. In such cases, a decision needs to be made whether to simply fill the cracks or to provide other corrosion preventions. To address this issue, a method for evaluating the CR of steel bars after crack initiation is required. Several studies have experimentally evaluated the chloride-induced CR of the steel bar in cracked concrete [8–13]. These prediction models or factor analyses have been developed using polarization resistance (PR) monitoring.

However, few of them have had the accuracy verified by comparing the estimated corrosion weight loss (CWL) with actual CWL. The estimated CWL is obtained from the time integration of the CR, whereas the actual CWL is obtained by measuring the corrosion weight of a steel bar removed from the RC specimen. Law et al. [14] verified the accuracy of a PR method by actual CWL, but the PR method overestimated the CWL, especially in chloride-induced corrosion. This was because macrocell corrosion had occurred and the predetermined evaluation area did not match the actual evaluation area. Liu and Weyers [2] compared CRs calculated using two types of linear PR method to the mean CR obtained from actual CWL. Both estimated CRs significantly differed from the actual mean CR. Jung et al. [3] verified the accuracy of a PR method using 11 steel bars in concrete corroded for 1 year, but the difference due to the corroded area was unclear. Especially for RC after bending cracking, corrosion tends to progress around the transverse crack [11]. Thus, if a corrosion prediction model is proposed based on PR monitoring without accuracy verification, it may differ greatly from the actual CWL. It is necessary to clarify the verification method by performing the PR method experimentally. In addition, few studies have evaluated the effect of crack repair on the CR, and applicability of PR methods to such specimen remains unclear.

In this study, we measured the time-variant CR of the steel bar in cracked and crack-repaired concrete every one to three months over three years in an accelerated corrosion environment. An alternating current (AC) impedance method, one of the PR methods, was used for the CR monitoring. To confirm accuracy, the corroded area and CWL of the steel bars were measured. Then, the trend of the CR with time of the steel in such concrete was proposed.

2. Experimental Procedure

2.1. Specimens

A corrosion experiment was conducted to consider the effect of cracks and crack repair on the corrosion progress using RC specimens. Figure 1 shows the geometry of the RC specimens and the arrangement of the electrodes when we applied an AC impedance method.

Figure 1 RC specimens and application of the AC impedance method

Each specimen was a 100 mm × 100 mm × 376 mm RC prism containing one 400-mm long deformed steel bar (SD295A) with a diameter D = 10 mm. This steel bar was cast in the specimen such that the minimum depth to the concrete surface c = 30 mm. The test length of the bar was 300 mm, with the remainder at each end coated with epoxy resin. A coaxial cable was connected to the steel bar. Table 1 provides the concrete mix design and Table 2 provides the experimental parameters of the specimens.

Table 1
Concrete mix design of the specimens

Max diameter of aggregate (mm)	Slump (cm)	Air content (%)	W/C (%)	Fine aggregate content (%)	Unit quantity (kg/m^3)						Compressive strength (N/mm^2)
					Water	Cement	Fine aggregate	Coarse aggregate	AE water reducing agent	AE auxiliary	
13	10 ± 2.5	4.5 ± 1.5	55	47	188	342	793	946	0.855	1.368	36.7

Table 2
Experimental parameters of the specimens

Specimen	Crack width (mm)	Crack repair	Quantity
N-N	0	No	6
0.2C-N	0.2	No	4
0.4C-N	0.4	No	6
0.6C-N	0.6	No	4
0.2C-R	0.2	Yes	2
0.4C-R	0.4	Yes	6
0.6C-R	0.6	Yes	2

The RC specimens were cured by seal in the laboratory for 28 d at a temperature of 20°C and 70% relative humidity. After curing, compressive strength tests were conducted on 3 cylindrical specimens with a 100 mm diameter and 200 mm height in accordance with JIS A 1108 [15], and the average compressive strength was 36.7 N/mm^2. According to the experimental parameters reported in Table 2, a transverse crack was introduced in the test surface of each concrete specimen by applying three-point bending. To check the crack width, a distortion (Pi) gauge was placed at the center of the test surface in line with the steel bar inside the concrete. After the specimen was unloaded, each crack width was confirmed to be within ± 10% of the desired value.

Then, cracks of some specimens were repaired using an epoxy resin as per the experimental parameters. To ensure that the penetration of salinity progressed from only the test surface of the concrete, coal tar epoxy resin was coated on the remaining 5 surfaces. Then, the specimens were exposed to an environmental load device to accelerate corrosion. This device sprayed the specimens with 3% NaCl water solution for 3 min once a day, while maintaining the surrounding air at 40°C and 80% relative humidity.

2.2. AC impedance measurement procedure

Linear PR method has been used because of its simplicity of measurement and ease of interpretation, but with the recent miniaturization and enhancement of equipment, the AC impedance method is also being applied in many cases [16, 17]. The method measures the target sample by changing the current frequency using a potentiometer/ galvanostat with a frequency response analyzer (FRA). The impedance (Z) plotted on the complex plane are called Nyquist plots. Thus, Z is calculated as

$$Z = Z_{\mathrm{Re}} + jZ_{\mathrm{Im}} \left(j = \sqrt{-1}\right) \quad (1)$$

where Z_{Re} is the real value and Z_{Im} is the imaginary value of Z. An equivalent circuit model of RC is assumed as shown in Fig. 2(a), and Fig. 2(b) shows examples of Nyquist plots in our experiment. This model is the simplest among the various proposed models for the RC specimen. The capacitance (C_{dl}) and apparent PR ($R_{\mathrm{p,app}}$) are formed at the interface between the steel and concrete because the anions and cations are separated by a potential difference, known as an electric double layer [18]. This ion flow is similar to a parallel circuit comprising C_{dl} and $R_{\mathrm{p,app}}$.

Here, $R_{p,app}$ is the PR not considering the measurement area of the steel. The PR (R_p) can be calculated by multiplying the $R_{p,app}$ by the measurement area (A) of the steel through which the measurement current flows. Also, the solution resistance of concrete (R_s) is expressed as an additional resistance. The impedance property of the equivalent circuit model is expressed as

$$\left(Z_{\mathrm{Re}} - R_s - \frac{R_{p,app}}{2}\right)^2 + Z_{\mathrm{Im}}^2 = \left(\frac{R_{p,app}}{2}\right)^2$$

2

.

A semicircle with a radius of $R_p/2$ and center coordinates of (R_s+ $R_{p,app}/2$, 0) is shown in the complex plane, as shown in Fig. 2(b). Using this procedure, the AC impedance method is able to calculate the $R_{p,app}$ and R_s separately.

Figure 2 Examples of calculation of $R_{p,app}$ and R_s using the Nyquist plot: (a) equivalent circuit model; (b) examples of Nyquist plots

For our experiment, the steel bar in the specimen was used as the working electrode (WE), a 50 mm × 100 mm thin stainless-steel board (SUS304) was used as the counter electrode (CE), the Pb reference electrode (PRE) was the reference electrode (RE), and a high-water-absorption sponge made of polyvinyl alcohol was placed between the CE and the concrete surface, and between the RE and the concrete surface. Note there are two types of CE: one with and one without guard rings. In this study, the CE without guard rings was applied by adopting the experiment setup employed by Liu and Weyers [2], who stated that the PR method without guard rings was able to estimate the CR more accurately. The CE was located at the center of the concrete surface and the RE was located 10 mm from the edge of the CE. The concrete was wet (6–8% water content) in every measurement.

The measurement conditions were as follows. The potential difference was ΔV = ± 30 mV. The frequency range of the current was 10 mHz to 10 kHz. The $R_{p,app}$ and R_s, were calculated by performing curve fitting using analytical software for electrical measurements. The $R_{p,app}$ was measured every one to three months until the specimens were split for verification. This type of approach is often referred to as monitoring.

2.3. Calculation of CR and estimated CWL

From the apparent PR ($R_{p,app}$) obtained from the procedure described in the previous section, the corrosion current density i_{corr} (μA/cm^2) can be calculated as follows:

$$i_{corr} = B \cdot \frac{1}{R_p} = B \cdot \frac{1}{R_{p,app} \cdot A}$$

3

,

where B is the constant value (mV) proposed by Stern and Geary [19], R_p is the PR (kΩ·cm^2 (= $R_{p,app}$ × A)), $R_{p,app}$ is the apparent PR (kΩ), and A is the measurement area of the steel (cm^2). The value of B has been calculated experimentally, and some studies have determined it to be 26 mV [20–22], so we used this value in this study. Subsequently, the corrosion current density i_{corr} can be converted to the CR (mg/cm^2/d) by

$$CR = \frac{\alpha}{1000} \cdot \frac{M}{2F} \cdot i_{corr}$$

4

,

where M is the atomic weight of iron (= 55.85 g/mol), F is the Faraday constant (= 96,485 C/mol), and α is a constant that converts from days to seconds (= 8.64×10^4 s/d). This equation is based on a half-reaction equation in which iron releases electrons to become divalent iron ions, and calculates the dissolution rate of iron from the electrons generated. Based on this procedure, the PR method can be used to quantitatively evaluate the CR. One of the problems of the PR method is the change in the measurement area owing to the current dispersion in the concrete. Previous researchers conducted a current-dispersion analysis of concrete before crack initiation using the finite-element method [23], but only a few experimental studies have considered the current dispersion of RC specimens.

The CWL was then calculated from the monitoring results by

$$G = \sum_{t=1}^{t_f} \frac{1}{2} \cdot \left(CR_{(t)} + CR_{(t-1)}\right) \cdot \left(T_{(t)} - T_{(t-1)}\right)$$

5

,

where G is the CWL per unit surface of the steel (mg/cm^2), t is the number of measurements, t_f is that of the last measurement, $R_{p,app(t)}$ is the apparent PR of the t-th measurement (kΩ), and $T_{(t)}$ is the time from the start of exposure to the t-th measurement (d). Here, we determined $CR_{(0)}$ = 0 (mg/cm^2/d) and $T_{(0)}$ = 0 (d). Eq. (5) first calculates the area of the trapezoid enclosed by the interval between two consecutive points in time and their corresponding PR values. Thereafter, the CWL is calculated by integrating the area of this trapezoid over the entire corrosion time; this is called the estimated CWL.

2.4. Measurement of actual CWL

The procedure for measuring the actual CWL was applied as follows. First, following the exposure period, each specimen was divided into two parts by split loading at the steel bar location. The steel bar was then removed from inside the specimen, and the corroded area and the CWL were measured. Figure 3 shows the calculation procedure of the corrosion area ratio. Six photographs of the removed steel bar, rotated every 60° around its longitudinal axis, were obtained to determine the corroded area. Then, the corroded and non-corroded areas were binarized using the Image J area calculation software [24]. The corrosion area ratio r_{ca} (%) was calculated by

$$r_{ca} = 100 \cdot \frac{S_{corr}}{S}$$

6

,

where S is the total test area of the steel, calculated by multiplying half of the diameter of the bar, D/2, by the test length (30cm) for all six surfaces, and S_{corr} is the total corroded area, calculated by binarizing the non-corroded and corroded areas in the six images based on the color of the bar, given that the color of a rusted area is changed from silver to red or black.

Figure 3 Calculation procedure of the corrosion area ratio

The weight loss due to corrosion was measured by weighing the steel after the corrosion products were removed by immersion in an aqueous solution of 10% diammonium hydrogen citrate at 60°C for approximately 24 h, as per JCI-SC1 [25]. Thereafter, the CWL per unit area at the corroded area ΔW (mg/cm^2) was calculated by

$$\Delta W = \frac{(W_0 - W) - W_p \cdot (100 - r_{ca})/100}{S_{corr}}$$

7

,

where W_0 is the weight of the steel before placement (mg), W is the weight of the corroded steel after removing the rust (mg), and W_p is the weight of the mill-scale on the steel (mg). Mill-scale is an oxidized film that forms on the surface during the manufacture of a steel bar.

3. Results

3.1. Comparison between estimated and actual CWL

The actual CWL is compared to that estimated by the PR monitoring in Fig. 4. As a consideration of the measurement area (A) of the PR method, Fig. 4(a) shows the comparison when A is set as the total test area (S), whereas Fig. 4(b) shows the comparison when A is set as the total corroded area (S_{corr}) of each specimen. The figure shows each specimen type using different plot points, and straight lines passing through 0 and 400 mg/cm^2 representing $\Delta W = G$, $\Delta W = 0.5 \times G$, and $\Delta W = 2.0 \times G$. The C-N and C-R specimen types each had three different crack widths (0.2, 0.4, and 0.6 mm), but are not distinguished here. Thus, the G underestimated the ΔW by a factor of two or more when S was used, whereas the G estimated ΔW with relatively good accuracy regardless of the specimen parameters when S_{corr} was used. The results clarify that the measurement area A was almost equal to the corroded area S_{corr}.

Figure 4 Comparison of actual and PR-estimated CWL: (a) Comparison when A is set as the total test area; (b) Comparison when A is set as the total corroded area

For consideration of the relationship between the measurement area A and corroded area S_{corr}, Fig. 5 shows a conceptual diagram of the current dispersion in the case of localized corrosion. When the steel bar inside the concrete is almost non-corroded, the current disperses over its

entire surface because the PR of the steel–concrete interface is uniform. However, in the case of localized corrosion, the measurement current is concentrated in the area with low PR, or corroded area. The results and consideration indicate that the corroded area should be calculated in addition to the CWL for accuracy verification. In addition, the AC impedance method is highly accurate and feasible for the cracked and crack-repaired concrete specimens.

In this experiment, the concern is that many specimens underestimated the CWL. It was found that 80% of the specimens had $\Delta W > G$, and 40% of the specimens had $\Delta W > 2.0 \times G$. There are two possible reasons for this. Firstly, it is difficult to detect the minor corrosion occurrence such as point rust by the AC impedance method, while the actual CWL was calculated to be large due to the small corrosion area ratio. On this basis, there were a great number of specimens that were underestimated at 70 mg/cm^2 or less. Secondly, the measurement area was set as the corroded area of the steel bar at the time of splitting the specimens. This method can accurately determine the CR at the split time. However, the corroded area generally increases with the corrosion progress, and therefore, the corroded area during the exposure period is expected to be smaller than that at the split time. In other words, CR may be measured lower than the actual rate due to the determined measurement area being larger than the actual corroded area during the exposure period. How to effectively set the actual corroded area during the exposure presents an important avenue for a future work.

Figure 5 Conceptual diagram of current dispersion in case of localized corrosion

3.2. Time-variant CR

Figure 6 shows the mean time-variant corrosion current density (I_{corr}) of specimens 0.2C-N, 0.4C-N, and 0.6C-N calculated by the AC impedance method. I_{corr} can be converted to CR by simply multiplying by a constant as shown in Eq. (4). For each factor, the CR increased rapidly for approximately 50 weeks after exposure and thereafter decreased slightly before finally remaining at an almost constant value. To consider the difference of these CRs due to different factors, Fig. 7 shows the mean data of the current densities and their standard deviation after 50 weeks for 0.2C-N, 0.4C-N, and 0.6C-N. The large standard deviation compared to the difference in the mean values indicates that there is no significant difference for the evaluated crack range (0.2–0.6 mm). The reason for the slight CR decrease from 60–80 weeks to after 100 weeks was thought to be that oxygen and water from outside were prevented from entering due to the accumulation of corrosion product on the steel surface. Yuan et al. [5] also considered that the CR after the concrete cracking would become steady because corrosion products gradually filled up the cracks and oxygen access retarded.

Figure 6 Time-variant corrosion current density of the C-N specimens

Figure 7 Mean corrosion current values after 50 weeks of each factor

Figure 8 shows the mean time-variant corrosion current density for the C-R and N-N specimens. The corrosion can be observed to have occurred approximately 20–30 weeks after exposure as the chloride ions introduced by the salt spray gradually penetrated the concrete. Furthermore, presence or absence of cracks on the surfaces of the specimens were observed after each PR measurement, then the occurrence of corrosion cracks was confirmed after approximately 70–80 weeks. The CR immediately after the appearance of cracks was approximately 2–3 times higher than the previous CR owing to the rapid increase in the chloride ion and oxygen supply through the cracks. Focusing on the plot in Fig. 8, the CR can be observed to increase almost linearly between corrosion initiation and crack initiation. Indeed, it was determined that the CR was low immediately after corrosion initiation during the progress period, but increased with time as the chloride ion content in the concrete gradually increased at the location of the steel bar.

Figure 8 Time-variant corrosion current density of the C-R and N-N specimens

Comparing the results in Figs. 6 and 8, the cracked RC specimens in a severe salt environment reached a high CR after 50 weeks of exposure, indicating that corrosion occurred and progressed early. This is attributed to the faster salt penetration and higher oxygen permeability facilitated by the presence of cracks. Furthermore, it took a long time for corrosion to occur in both the N-N and C-R specimens, and their subsequent increases in CR were both minimal. It was therefore shown that corrosion initiation and progression could be inhibited in specimens with bending cracks to the same extent as in specimens without cracks by repairing the cracks before corrosion initiation.

4. Discussion

The contributions of this work are detailed through a comparison of the results of this study with those of previous studies. It is well-known that the PR method can quantify the CR of RC specimens without concrete cracks [19]. There have also been several examples of the application of electrochemical methods to specimens after cracking [7, 8]. However, few studies have confirmed the accuracy of their results by comparing the actual CWL with that obtained from the time-integrated value of the CR after crack initiation or crack repair. Thus, an important contribution of this study is its empirical demonstration of the applicability of the AC impedance method to RC after being cracked and repaired.

The corrosion initiation time and time-variant CR of steel bars in concrete vary depending on the presence or absence of cracks. Figure 9 shows conceptual diagrams of the time-variant CR, as determined by monitoring. Figure 9(a) shows the results of a specimen with bending cracks, and Fig. 9(b) shows the results for a specimen without cracks or a specimen with the cracks repaired.

Figure 9 Time-variant CR of steel bars inside (a) cracked concrete and (b) uncracked and crack-repaired concrete

Some previous studies have shown that the CR is higher when the crack width is larger [26, 27] whereas others have shown that the crack width is almost unrelated to the CR [11, 12]. In this study, the crack width was found to be irrelevant in the range of 0.2–0.6 mm. The reason is that degradation factors such as chloride ions, water, and oxygen can easily penetrate the concrete through the crack, regardless of its width. Sangoju et al. [11] and Okada and Miyagawa [12] suggested that the type of concrete affects the CR more than the crack width. Therefore, it remains necessary to conduct a parametric study of the time-variant CR under various environmental and concrete conditions to develop a versatile CR prediction method.

Furthermore, our results demonstrated that the increase in CR after crack initiation does not continue with time. Japan Concrete Institute (JCI) [27] and our previous research [28] proposed the prediction model with continuously increasing CR. Rather, as shown by Otieno et al. [8], Chen and Mahadevan [29], and Cao et al. [30], the increase in CR gradually slows with time until eventually reaching a constant value. We verified such time-variant CR through accuracy verification of the CWL.

If the AC impedance method is conducted after identifying the areas where the CR should be obtained, the deterioration state of the structure can be efficiently quantified. In this study, the AC impedance method was applied to a series of specimens of a single geometry design. To apply this method to actual RC structures, it will be necessary to take into account various factors such as the steel bar length, concrete cover, electrical resistance of the concrete, and shape of the CE. In addition, it is considered difficult to apply the AC impedance method to structures that have deteriorated to the extent that the concrete cover has delaminated after cracking, so it remains necessary to clarify the types of deterioration to which it can be applied. Thus, the application of the AC impedance method to the maintenance of existing structures still has many issues that need to be addressed, and further studies are necessary.

In summary, this study provides valuable information describing methods for the measurement of corrosion deterioration and the prediction of corrosion progress.

5. Conclusions

In this study, AC impedance measurements for RC specimens with and without cracks and crack repairs were conducted every one to three months for three years. In addition, the corrosion area and CWL of the steel were measured for verification. The following conclusions were drawn from the results of this study:

(1) The results clarify that the measurement area of the AC impedance method was almost equal to the corroded area, which indicates that the corrosion area should be calculated in addition to the CWL for accuracy verification.

(2) The results show that the AC impedance method can be applied to cracked and crack-repaired concrete for measuring time-variant CR.

(3) The PR monitoring results clarified that the CR increased over a short period of time following the appearance of a crack, but this increasing trend gradually slowed. Thus, CR eventually reached an approximately constant value.

(4) The repair of flexural cracks before the onset of corrosion reduced the change in CR with time to the same level as that of the specimens without cracks.

In future research, case studies of the time-variant CR under various environmental and material parameters will be conducted to develop a more versatile prediction equation. Furthermore, the finite-element method and other analytical methods will be applied to clarify the current dispersion characteristics when localized corrosion occurs, expanding the applicability of the proposed AC impedance method.

Declarations

Competing Interests

There are no competing interests.

Funding

This research did not receive any specific grant from funding agencies in the public, commercial, or not-for-profit sectors.

Abbreviations

alternating current (AC), corrosion rate (CR), corrosion weight loss (CWL), counter electrode (CE), frequency response analyzer (FRA), Pb reference electrode (PRE), polarization resistance (PR), reinforced concrete (RC), water-binder ratio (W/B), reference electrode (RE), working electrode (WE)

References

[1] Yalçyn H, Ergun M (1996) The prediction of corrosion rates of reinforcing steels in concrete. Cem Concr Res 26:1593–1599. https://doi.org/10.1016/0008-8846(96)00139-1

[2] Liu T, Weyers RW (1998) Modeling the dynamic corrosion process in chloride contaminated concrete structures. Cem Concr Res 28:365–379. https://doi.org/10.1016/S0008-8846(98)00259-2

[3] Jung W-Y, Yoon Y-S, Sohn Y-M (2003) Predicting the remaining service life of land concrete by steel corrosion. Cem Concr Res 33:663–677. https://doi.org/10.1016/S0008-8846(02)01034-7

[4] Vu KAT, Stewart MG (2000) Structural reliability of concrete bridges including improved chloride-induced corrosion models. Struct Saf 22:313–333. https://doi.org/10.1016/S0167-4730(00)00018-7

[5] Yuan Y, Ji Y, Jiang J (2009) Effect of corrosion layer of steel bar in concrete on time-variant corrosion rate. Mater Struct 42:1443–1450. https://doi.org/10.1617/s11527-008-9464-9

[6] Jiang J, Yuan Y (2012) Prediction model for the time-varying corrosion rate of rebar based on micro-environment in concrete. Constr Build Mater 35:625–632. https://doi.org/10.1016/j.conbuildmat.2012.04.077

[7] Jiang J, Yuan Y (2013) Development and prediction strategy of steel corrosion rate in concrete under natural climate. Constr Build Mater 44:287–292. https://doi.org/10.1016/j.conbuildmat.2013.03.033

[8] Otieno M, Beushausen H, Alexander M (2016) Chloride-induced corrosion of steel in cracked concrete – Part I: Experimental studies under accelerated and natural marine environments. Cem Concr Res 79:373–385.

https://doi.org/10.1016/j.cemconres.2015.08.009

[9] Otieno M, Beushausen H, Alexander M (2016) Chloride-induced corrosion of steel in cracked concrete—Part II: Corrosion rate prediction models. Cem Concr Res 79:386–394. https://doi.org/10.1016/j.cemconres.2015.08.008

[10] Otieno M (2017) Sensitivity of chloride-induced corrosion rate of steel in concrete to cover depth, crack width and concrete quality. Mater Struct 50:1–10. https://doi.org/10.1617/s11527-016-0916-3

[11] Sangoju B, Gettu R, Bharatkumar BH, Neelamegam M (2011) Chloride-induced corrosion of steel in cracked OPC and PPC concretes: Experimental study. J Mater Civ Eng 23:1057–1066. https://doi.org/10.1061/(ASCE)MT.1943-5533.0000260

[12] Okada K, Miyagawa T (1980) Chloride corrosion of reinforcing steel in cracked concrete. In: Malhotra M (ed.), SP-65, performance of concrete in marine environment. ACI, p 237–254

[13] Du F, Jin Z, She W, Xiong C, Feng G, Fan J (2020) Chloride ions migration and induced reinforcement corrosion in concrete with cracks: A comparative study of current acceleration and natural marine exposure. Constr Build Mater 263. https://doi.org/10.1016/j.conbuildmat.2020.120099, 120099

[14] Law DW, Cairns J, Millard SG, Bungey JH (2004) Measurement of loss of steel from reinforcing bars in concrete using linear polarisation resistance measurements. NDT E Int 37:381–388. https://doi.org/10.1016/j.ndteint.2003.11.003

[15] JIS A 1108 (2018) Method of test for compressive strength of concrete. Japanese Industrial Standards Committee (JISC)

[16] Orazem ME, Tribollet B (2017) Electrochemical impedance spectroscopy, 2nd edn. Wiley, Hoboken

[17] Rodrigues R, Gaboreau S, Gance J, Ignatiadis I, Betelu S (2021) Reinforced concrete structures: A review of corrosion mechanisms and advances in electrical methods for corrosion monitoring. Constr Build Mater 269.

https://doi.org/10.1016/j.conbuildmat.2020.121240, 121240

[18] Andrade C, Alonso C (2004) Test methods for on-site corrosion rate measurement of steel reinforcement in concrete by means of the polarization resistance method. Mater Struct 37:623–643. https://doi.org/10.1007/BF02483292

[19] Stern M, Geary AL (1957) Electrochemical polarization: I. J Electrochem Soc 104:56–63. https://doi.org/10.1149/1.2428496

[20] Pech-Canul MA, Castro P (2002) Corrosion measurements of steel reinforcement in concrete exposed to a tropical marine atmosphere. Cem Concr Res 32:491–498. https://doi.org/10.1016/S0008-8846(01)00713-X

[21] Morris W, Vico A, Vazquez M, de Sanchez SR (2002) Corrosion of reinforcing steel evaluated by means of concrete resistivity measurements. Corros Sci 44:81–99. https://doi.org/10.1016/S0010-938X(01)00033-6

[22] Andrade C, Castelo V, Alomso C, Gonzalez JA (1984) The determination of the corrosion rate of steel embedded in concrete by the polarization resistance and AC impedance methods, Corrosion Rebar in Concrete. In: STP 906. ASTM International, West Conshohocken

[23] Yoshida H, Horiie Y, Yokota M (2016) Study on effects of heterogeneity on current propagation of reinforced concrete, JSCE. J Struct Eng 62a:12–22

[24] Abramoff, M.D., Magalhaes, P.J., Ram, S.J. (2004) Image processing with ImageJ. Biophotonics Int, 11: 36-42.

[25] JCI Standards 1977–2002 (2004) Japan Concrete Institute, 91–94.

[26] Ji Y, Hu Y, Zhang L, Bao Z (2016) Laboratory studies on influence of transverse cracking on chloride-induced corrosion rate in concrete. Cem Concr Compos 69:28–37. https://doi.org/10.1016/j.cemconcomp.2015.12.006

[27] Rehabilitation study committee's report of the concrete institute (1998). Japan Concrete Institute

[28] Kanemitsu T (2020) Evaluation of corrosion progress for reinforcing steel inside concrete after crack initiation or after crack repair using AC impedance method. J Soc Mat Sci Japan 69:921–928. https://doi.org/10.2472/jsms.69.921

[29] Chen D, Mahadevan S (2008) Chloride-induced reinforcement corrosion and concrete cracking simulation. Cem Concr Compos 30:227–238. https://doi.org/10.1016/j.cemconcomp.2006.10.007

[30] Cao C, Cheung MMS, Chan BYB (2013) Modelling of interaction between corrosion-induced concrete cover crack and steel corrosion rate. Corros Sci 69:97–109. https://doi.org/10.1016/j.corsci.2012.11.028

Figures

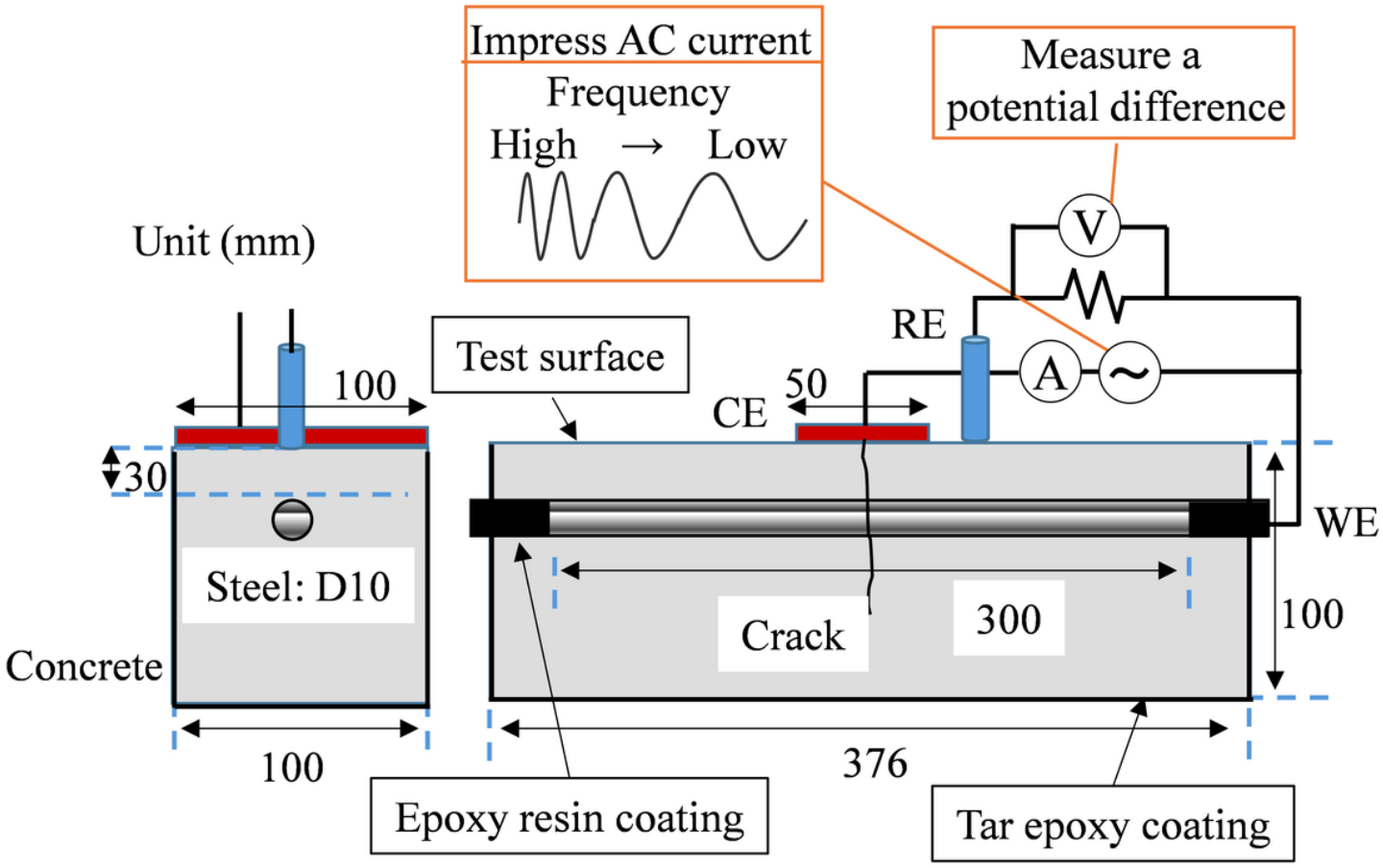

Figure 1

RC specimens and application of the AC impedance method

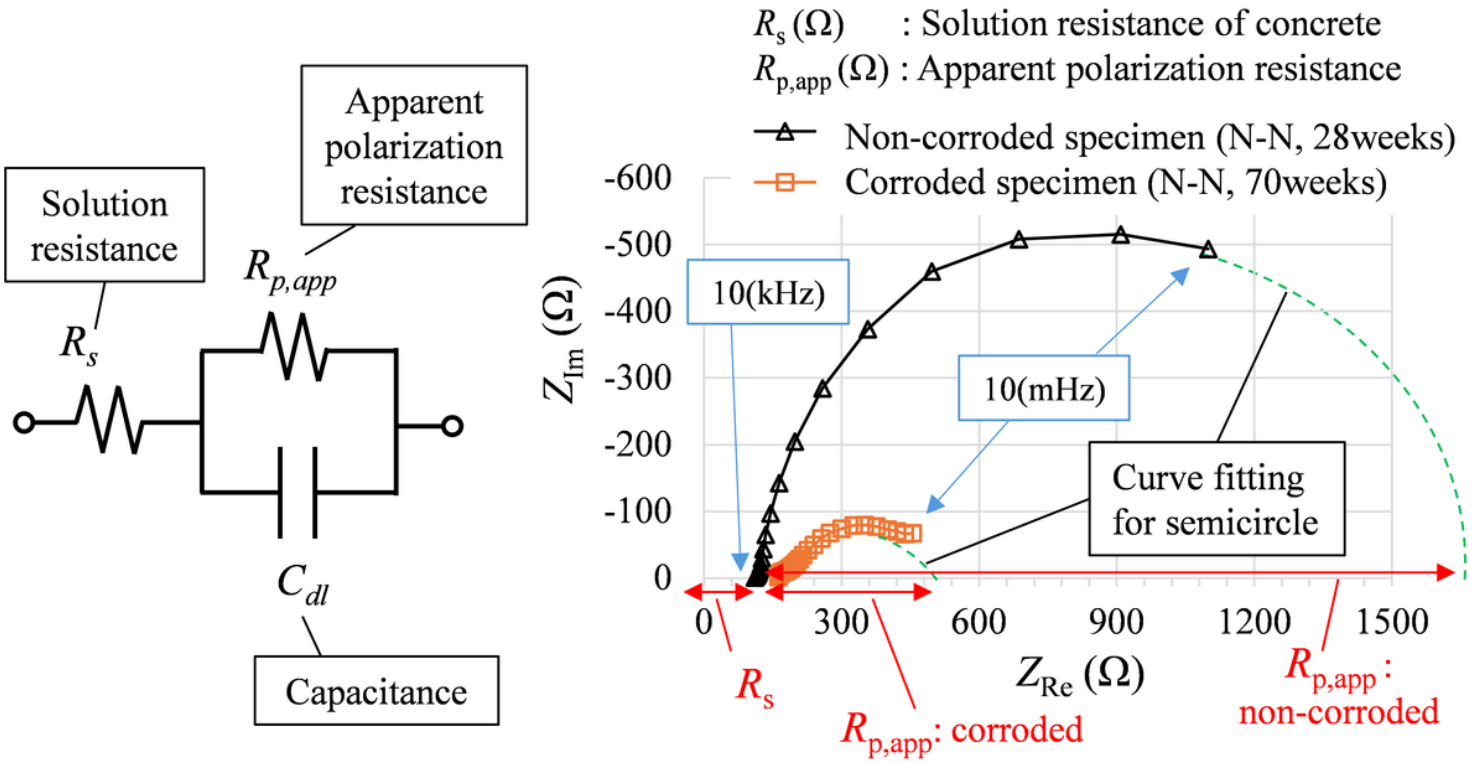

Figure 2

Examples of calculation of $R_{p,app}$ and R_s using the Nyquist plot: (a) equivalent circuit model; (b) examples of Nyquist plots

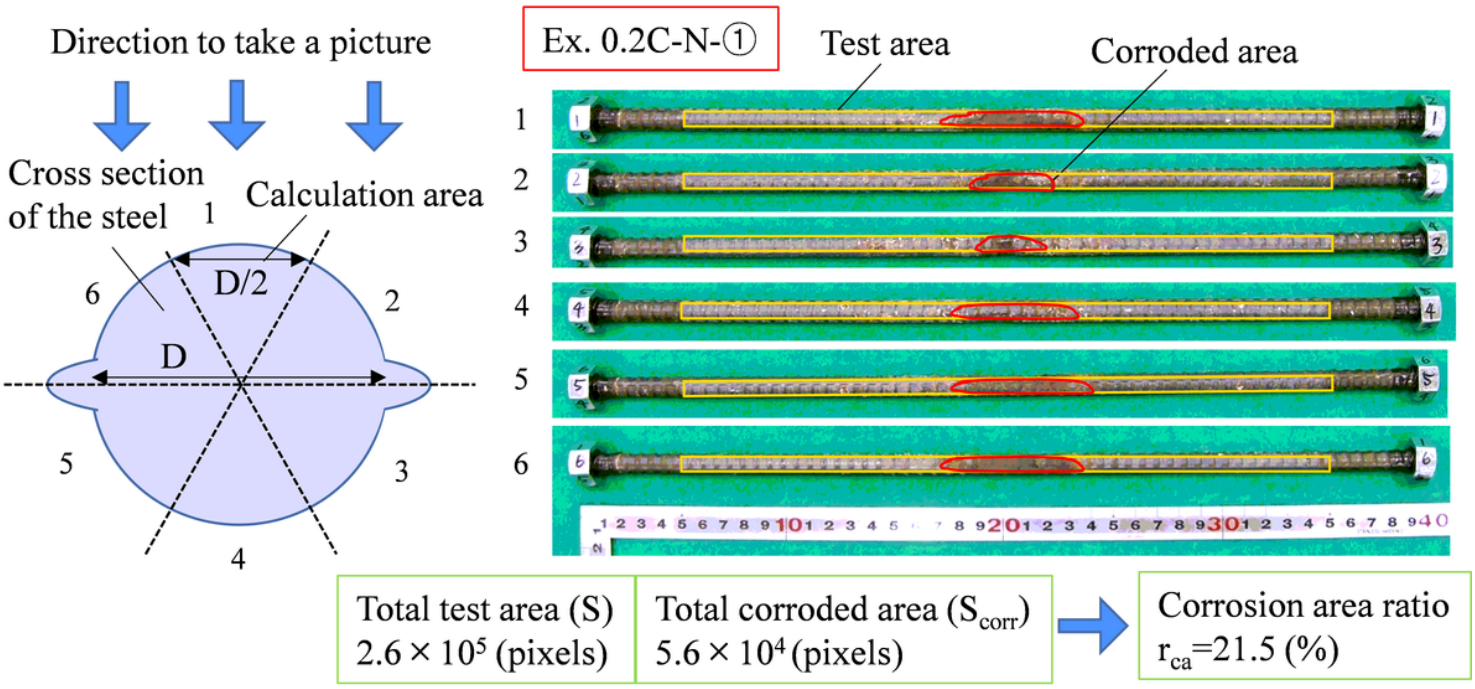

Figure 3

Calculation procedure of the corrosion area ratio

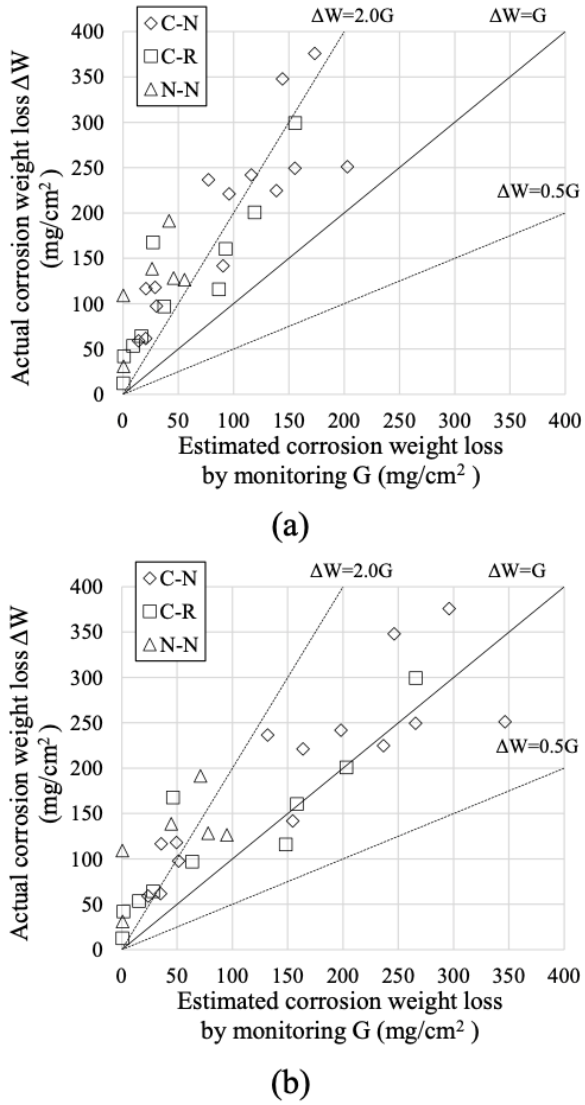

Figure 4

Comparison of actual and PR-estimated CWL: (a) Comparison when *A* is set as the total test area; (b) Comparison when *A* is set as the total corroded area

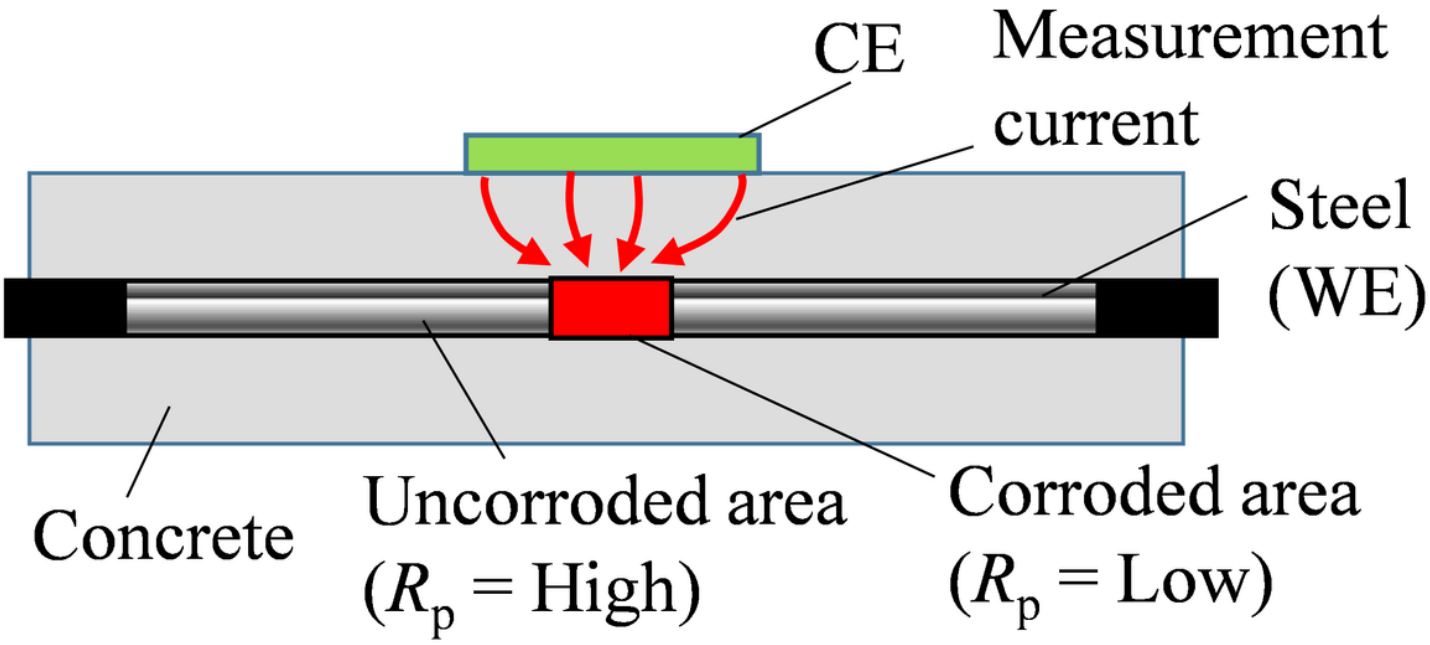

Figure 5

Conceptual diagram of current dispersion in case of localized corrosion

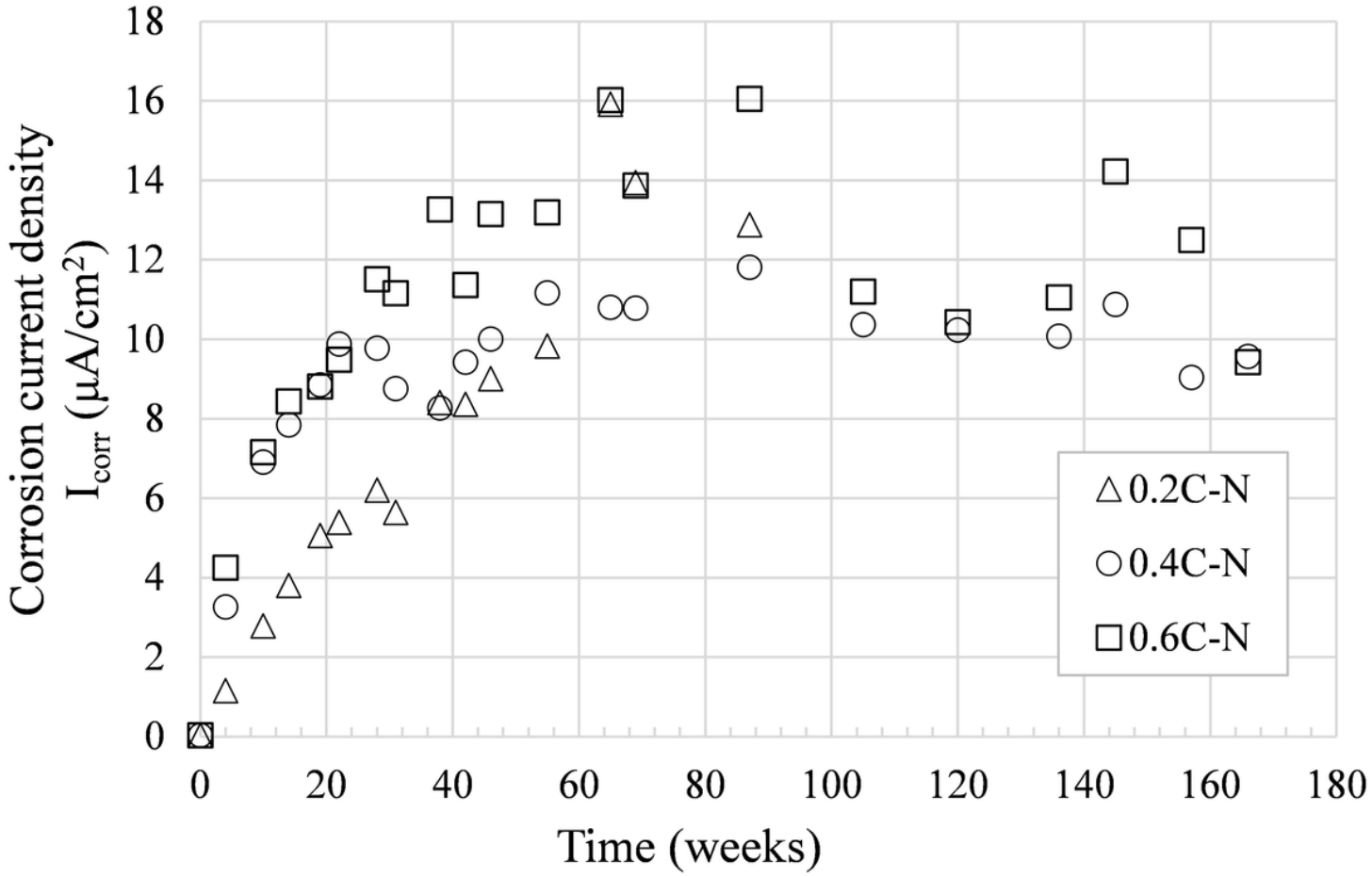

Figure 6

Time-variant corrosion current density of the C-N specimens

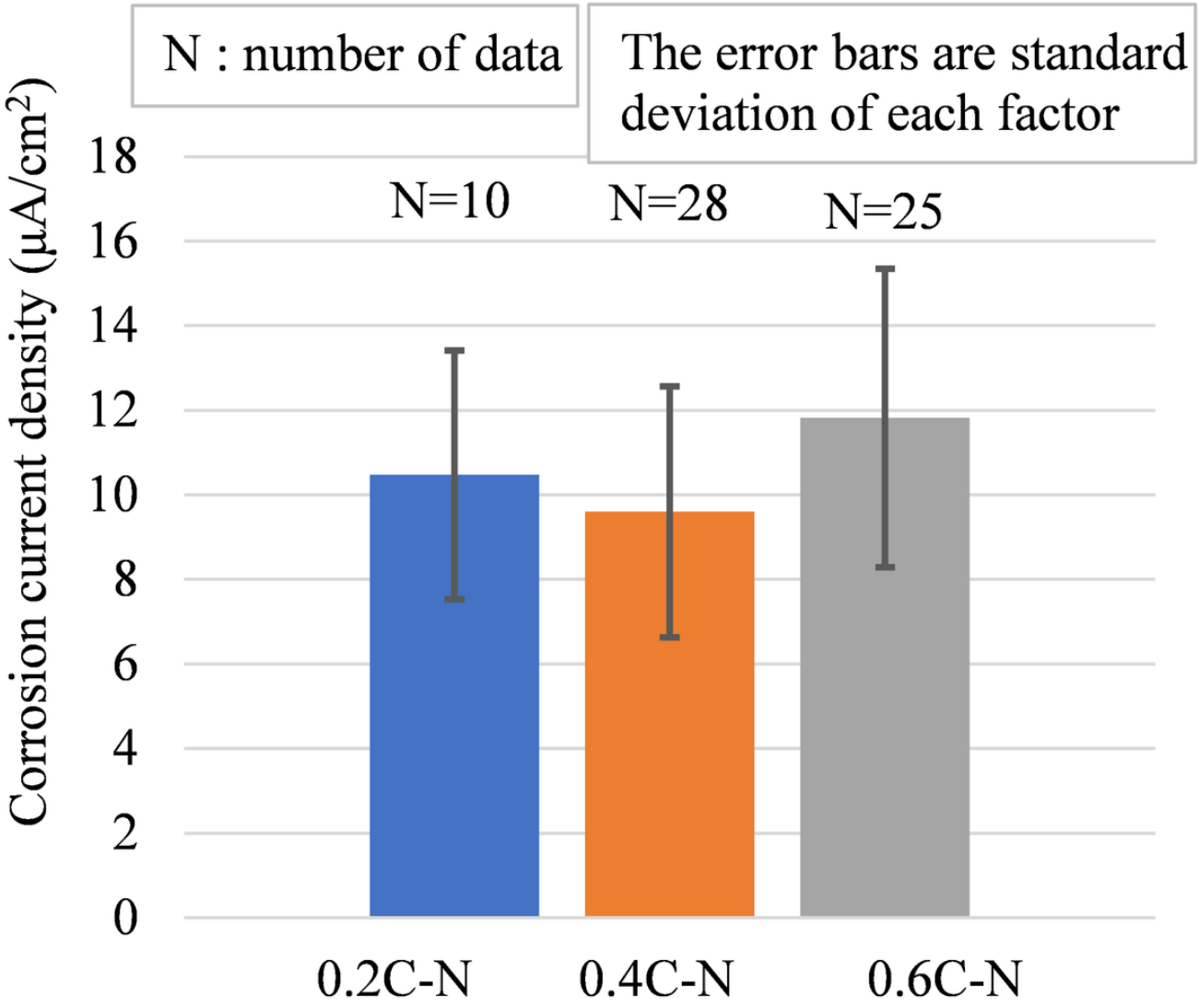

Figure 7

Mean corrosion current values after 50 weeks of each factor

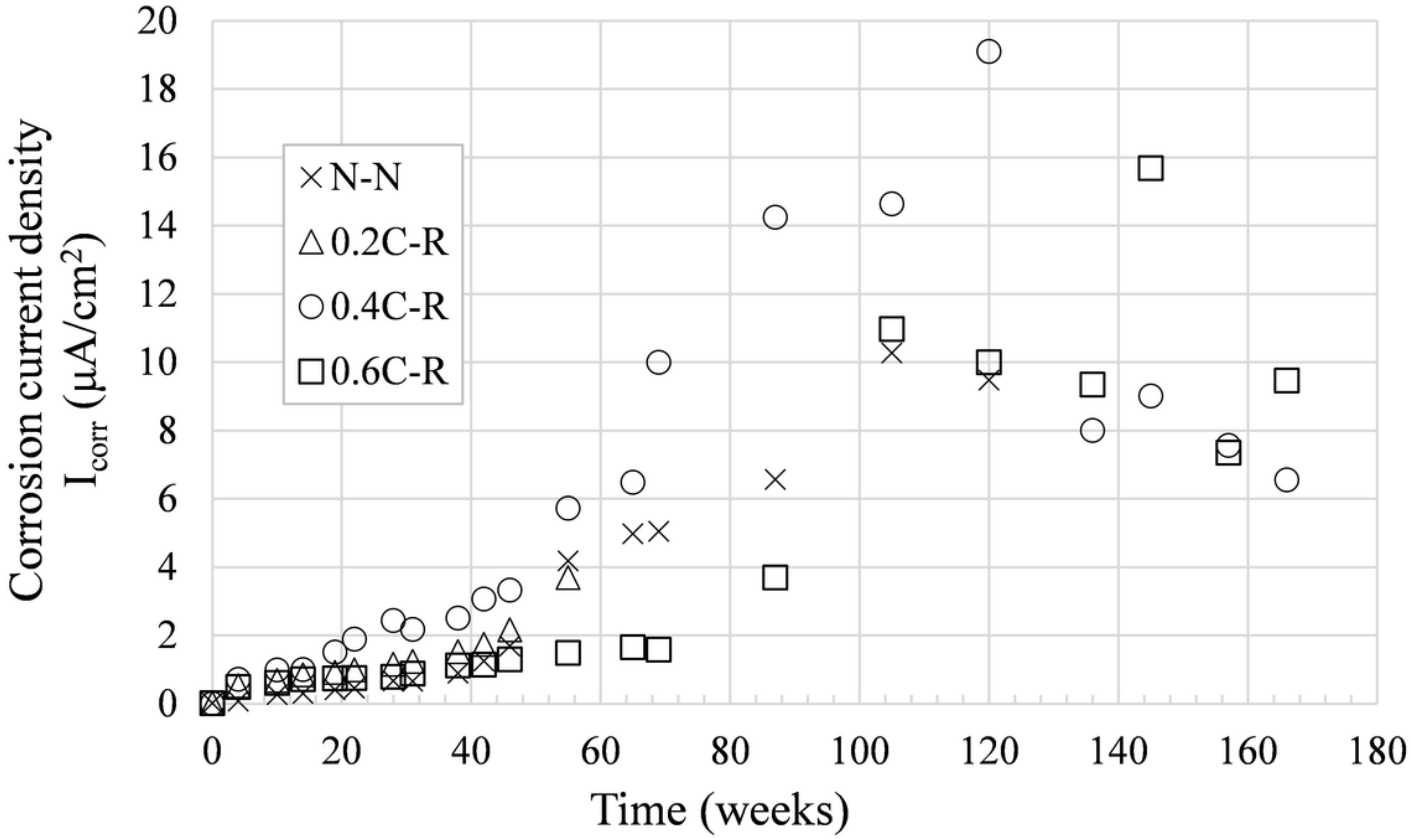

Figure 8

Time-variant corrosion current density of the C-R and N-N specimens

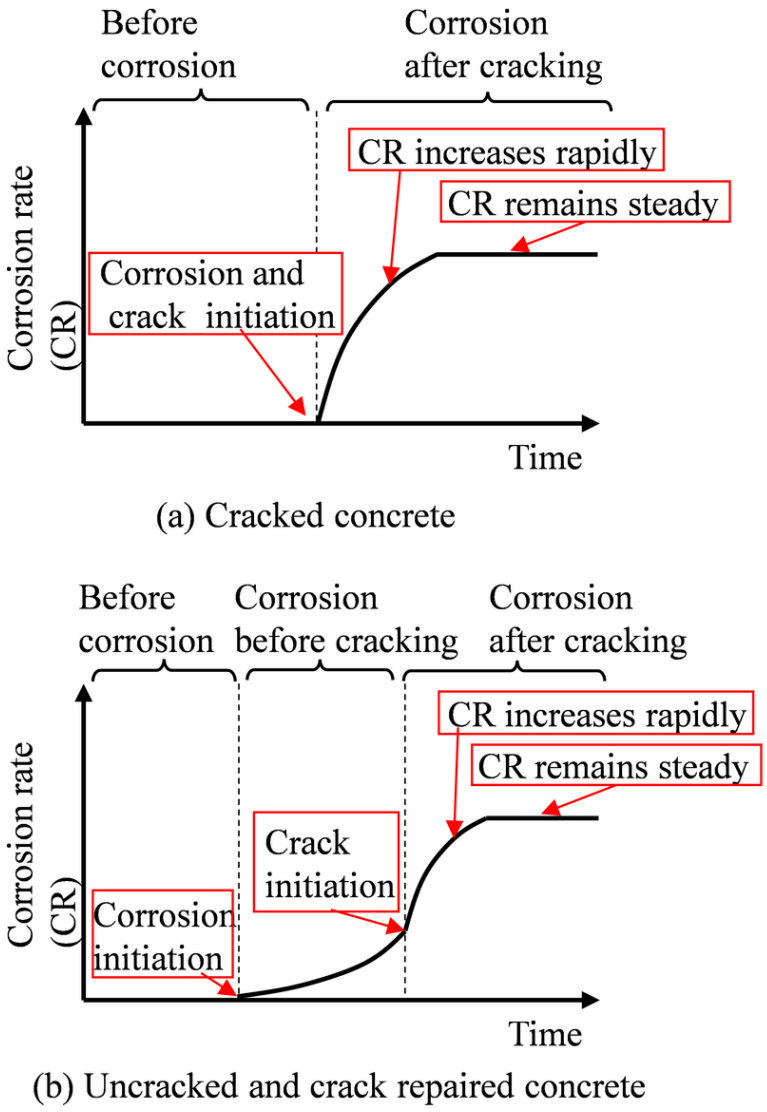

Figure 9

Time-variant CR of steel bars inside (a) cracked concrete and (b) uncracked and crack-repaired concrete

Supplementary Files

This is a list of supplementary files associated with this preprint. Click to download.

- DatasheetforMaterstructToshinoriKanemitsu.xlsx